Engineering Structures 161 (2018) 146–160

Contents lists available at ScienceDirect

Engineering Structures

journal homepage: www.elsevier.com/locate/engstruct

Strengthening of precast RC beam-column connections for progressive collapse mitigation using bolted steel plates

Yousef A. Al-Salloum*, Mohammed A. Alrubaidi, Hussein M. Elsanadedy, Tarek H. Almusallam, Rizwan A. Iqbal

Chair of Research and Studies in Strengthening and Rehabilitation of Structures, Department of Civil Engineering, College of Engineering, King Saud University, P.O. Box 800, Riyadh 11421, Saudi Arabia

ARTICLE INFO

Keywords:
Strengthening
Steel plates
Progressive collapse
Precast beam-column connection
Column removal scenario

ABSTRACT

Being one of the most critical scenarios in extreme events such as blast attacks, the progressive collapse of reinforced concrete (RC) structures has attracted the attention of structural engineering community. As precast concrete buildings are deficient in structural continuity, they are more vulnerable to progressive collapse than cast-in-situ RC buildings. Hence, effective rehabilitation techniques to upgrade beam-column joints in existing precast RC buildings for progressive collapse mitigation are needed. The goal of this study is to investigate the effectiveness of using bolted steel plates on the behavior of precast beam-column connections under sudden column-loss scenario. This study presents experiments involving one half-scale precast RC beam-column assembly, which represented the most prevalent types of existing precast beam-column joints in Saudi Arabia. One monolithic test specimen having continuity of top and bottom beam rebars was used for the sake of comparison. Another precast specimen similar to the control one was strengthened using bolted steel plates within the connection region. The progressive collapse scenario was simulated by removing the central column support and applying a sudden vertical load on this column at a rate of 100 mm/s until failure. The collapse load of both monolithic and strengthened specimens was predicted using a simplified section analysis procedure. The analysis was then used for some useful parametric studies in which the effect of different steel plate parameters on the response of test frames under middle column-loss scenario was investigated.

1. Introduction

In the last few decades, precast construction has become common in Saudi Arabia because of its high speed of construction. Buildings are extremely vulnerable to progressive collapses due to the loss of one or more columns caused by accidental events such as blast attacks. It is, therefore, important to study the behavior of precast concrete structures for progressive collapse to avoid catastrophic events. As precast buildings lack structural continuity and redundancy in the load paths, they are even more susceptible to progressive collapse than cast-in-situ monolithic buildings. Hence, effective and economical rehabilitation techniques to upgrade beam-column connections in existing precast concrete buildings for progressive collapse mitigation are needed.

The behavior of different types of precast RC beam-column joints has been investigated by numerous researchers [1–5]. In these studies, different designs for precast joints were studied which included: (i) connections using dowel rebars, (ii) dowel rebars with steel cleat angles, (iii) steel cleat angles with stiffeners, (iv) tie rods and steel plates, (v) use of cast-in-situ concrete in beam-column connection, (vi) bolted connections, (vii) composite connection with welding, etc. In these studies, the behavior of precast connections was evaluated in terms of load-displacement characteristics. The performance was then compared with their monolithic counterparts.

Savoia et al. [6] presented a complete and commented collection of cases of damage and collapse in precast concrete industrial buildings, observed during a series of field surveys after the 2012 Emilia earthquake in Northern Italy. They were selected among a total of about 2000 industrial RC precast buildings, whose structural characteristics and damage have been collected in a large database by the authors. The main causes of the collapses were vulnerabilities related to the structural characteristics of Italian precast buildings not designed with seismic criteria. In particular, these structures were typically built as an assembly of monolithic elements (roof elements, main and secondary beams, columns) in statically determinate configurations. The most common failure causes identified were: the absence of mechanical connectors between precast monolithic elements, the interaction of

* Corresponding author.
E-mail address: ysalloum@ksu.edu.sa (Y.A. Al-Salloum).

https://doi.org/10.1016/j.engstruct.2018.02.009
Received 21 May 2017; Received in revised form 13 December 2017; Accepted 1 February 2018
Available online 20 February 2018
0141-0296/

structural elements with nonstructural walls, the insufficient column bending capacity, the rotation of pocket foundations, the inadequacy of connections of external precast cladding walls to bearing elements (columns and beams), and the overturning of racks in buildings used as warehouses or in automated storage facilities.

One of the approaches to evaluate progressive collapse is to study the effects of sudden removal of vertical load-carrying members (such as a column) on the rest of the structure, and to check if any other alternate load paths do exist thereby arresting the damage initiation from propagating from one element to another. This notional column removal scenario adopted in many design codes and guidelines [7–12] is based on similar incidents occurred in the past such as the progressive collapse of a 22-story precast concrete apartment building at Ronan Point and the Alfred P. Murrah Building in Oklahoma City as result of an explosion [13,14]. There are many other examples of progressive collapse of buildings due to the damage of columns as result of vehicular impact such as the collapse of a building in New York City [15] and the parking structure of Isle of Capri casino [16]. Research on progressive collapse of structures was conducted by Peakau and Cui [17], Almusallam et al. [14,18], Allen and Schriever [19], Elsanadedy et al. [20], Baldridge and Humay [21], Choi and Chang [22], Al-Salloum et al. [23], Dat et al. [24], Bao et al. [25], and others. Kang and Tan [26] carried out an experimental study to investigate the behavior of precast RC beam-column test specimens under column-loss scenario. The beams and columns were joined together by cast-in-situ concrete topping above the two adjoining beams and the joint. The top longitudinal rebars passed through the joint continuously. The middle joint detailing involved 90° bend and lap-splice of bottom rebars. The specimens were tested to failure under quasi-static loads. It was concluded that the continuity of top reinforcement along with the cast-in-situ concrete topping led to the development of compressive arch action (CAA) and catenary action. However, the CAA and catenary action capacities were overestimated due to the rigid boundary conditions adopted in experiments.

In the past few years, a substantial research has been conducted on strengthening of deficient monolithic RC beam-columns joints using different techniques such as concrete jackets [27], steel jackets [28], fiber reinforced polymer (FRP) sheets [29–31] and textile reinforced mortar (TRM) strengthening [32]. However, strengthening of existing precast beam-column connections is a challenging task, which poses many practical difficulties. Da Fonseca et al. [33] carried out an experimental study on a small-scale precast concrete frame, comprising of two precast columns and one beam. The frame was loaded in two points of the beam until the cracks were observed in the beam. The beam-column joints were then strengthened using near surface mounted (NSM) CFRP strips embedded in the lateral concrete cover. The strengthened frame was reloaded until failure. Strengthened connections exhibited semi-rigid behavior and provided significant reduction in the beam mid-span deflection.

Gopinathan and Subramanian [34] studied experimentally the behavior of precast concrete frames under lateral loading. Two 1/4th scale, three-bay, five-story frames were cast. The first frame was monolithic that has been used as baseline for comparison; whereas the other one was precast RC frame. The beam-column joints in the precast frame were strengthened by specially designed steel bolts and L-angles via welding and bolting. The frames were subjected to lateral cyclic load until failure. The efficiency and performance of beam-column joints were studied and the behavior of precast frame was compared with the monolithic one. The ultimate base shear of the precast frame was about 90% of that of the monolithic frame. However, the story drift of the precast frame was 30% more than that of the monolithic frame.

de Freitas et al. [35] studied experimentally and numerically the use of bonded steel plates system and the sandwich steel plates system for stiffening the existing orthotropic bridge decks (OBD) for reducing the stress at the fatigue-sensitive details and thus extending the fatigue life of the decks. The reinforced deck panels were tested using realistic wheel loads. The results showed at least 40% stress reduction close to the fatigue-sensitive details in the reinforced decks. The two suggested reinforcement systems were shown to be the efficient lightweight solutions for stiffening the orthotropic bridge decks.

A search of literature indicates that even though there is considerable research on strengthening of monolithic RC beam-column joints using different techniques, but work on rehabilitation of precast RC beam-column connections is very limited. In fact, significant work on strengthening of precast RC beam-column joints for progressive collapse mitigation could not be found in the approachable references. Precast structures are widely used in residential and commercial buildings throughout the world. As a result, any collapse of precast structures would result in huge losses of life and property. For this reason, it is necessary to conduct research on the progressive collapse performance of precast structures and suggest methodologies to improve their behavior under such scenarios.

As mentioned previously, research on the progressive collapse potential of strengthened precast concrete beam-column connections could not be found. The lack of such research creates a challenge for such studies. The goal of this research is to investigate experimentally and analytically the progressive collapse risk of precast concrete beam-column joints strengthened using bolted steel plates. The progressive collapse was simulated in the testing by middle column loss scenario. In order to study the effectiveness of the strengthening technique, the results of the strengthened specimen were compared with both a reference unstrengthened precast specimen, which represented the most prevalent types of existing precast beam-column joints in Saudi Arabia, and a monolithic specimen with continuous top and bottom beam rebars.

2. Experimental program

2.1. Test matrix

The experimental program includes testing up to collapse a total of 3 half-scale beam-column connection sub-assemblages under vertical cyclic loading so as to provide the equivalent of severe progressive collapse damage. Details of the three test specimens are given in Figs. 1–3. It should be noted that in the designation of test specimens, the acronyms “PC” and “MC” denote precast concrete and monolithic concrete, respectively, the letters “C” and “S” symbolize control and strengthened specimens, respectively, and the acronym “SMF” stands for special moment frame with continuous top and bottom beam rebars. Out of the three specimens, the first one (PC-C) was an as-built control precast concrete specimen. This specimen was designed to represent the most common type of exiting precast beam-column connections in Saudi Arabia. Precast specimen PC-C was prepared with beam and column members cast individually and then assembled on test bed as is the norm in the field. The second specimen MC-SMF was monolithic with continuous top and bottom beam rebars through the joint region. The third beam-column connection specimen PC-S was the same as the precast control specimen, but it was strengthened using bolted steel plates within connection region. All specimens consisted of two-bay beams and three columns and were subjected to vertical dynamic loading that simulates a column-removal scenario due to extreme events such as blast attacks. The efficiency of the rehabilitation scheme was evaluated by comparing the experimental results of the tested specimens in terms of their mode of failure and load-displacement characteristics.

2.2. Test specimen details and assembly

The test specimens were designed to be half-scale of a prototype perimeter frame. The selected two-bay prototype frame was assumed to be a part of an eight-story commercial precast building located at a busy intersection of Riyadh. In the prototype building, the spans in both the

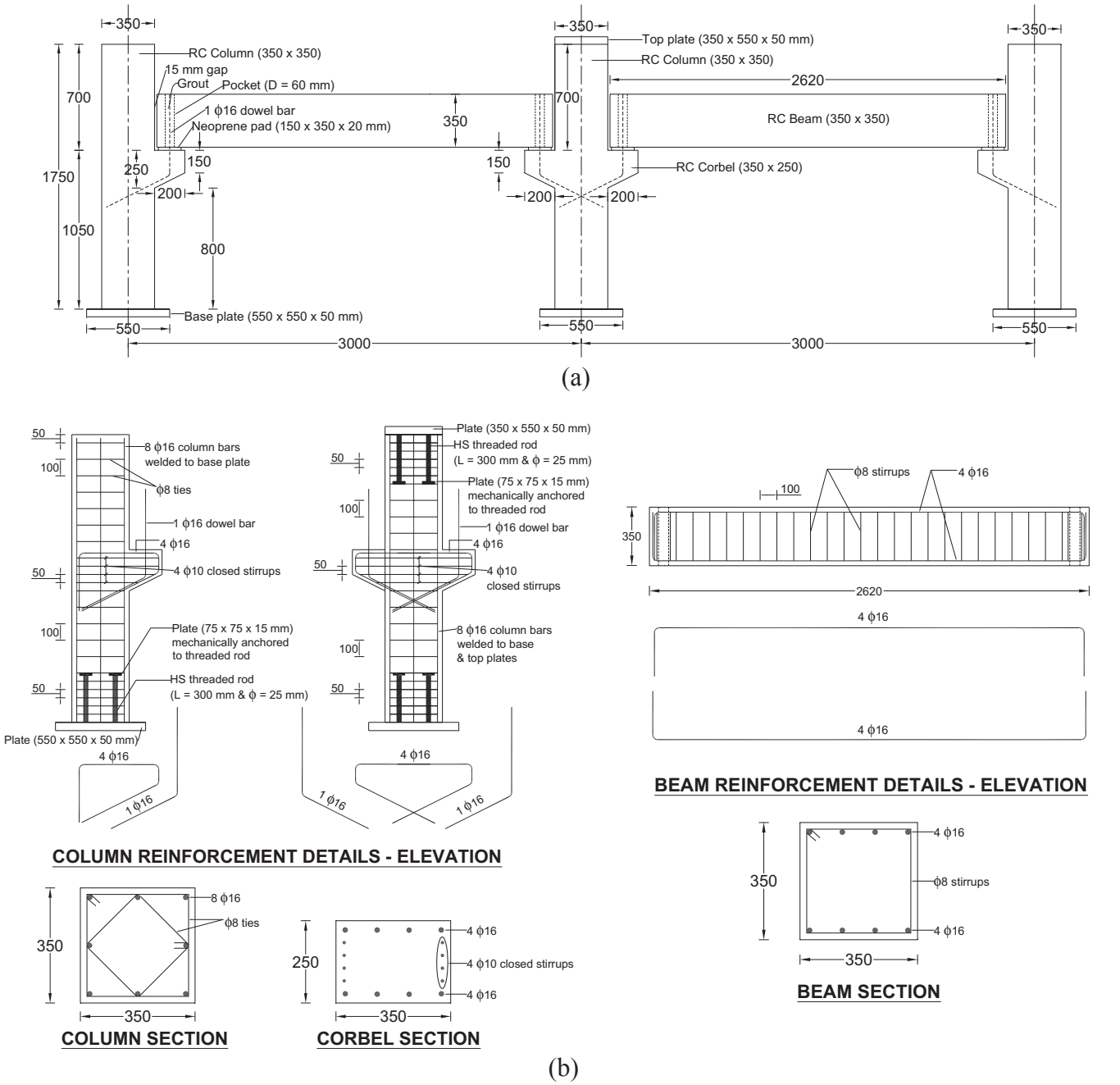

Fig. 1. Details of precast specimen PC-C (Note: All dimensions are in mm): (a) Test specimen; (b) Reinforcement details.

orthogonal directions were 6.0 m each. The live load used for the design was 4 kN/m^2 and the total superimposed dead load was 5 kN/m^2. A uniform line dead load of 16.3 kN/m was also used, which simulated the exterior non-structural façade components on the perimeter frames (230 mm thick precast exterior panels). The building was designed in conformance with the ACI 318-11 code [36]. The geometric dimensions for both the prototype frame and the specimens are presented in Table 1. The concrete dimensions and reinforcement details of the test specimens are depicted in Figs. 1–3. The two half-scale precast specimens PC-C and PC-S have the same concrete dimensions and reinforcement detailing. For the columns and the beams, section sizes of 350 × 350 mm were used and the corbels had section dimensions of 350 × 250 mm. The height of the column to the bottom of the beam was 1070 mm and the columns were made to rest on a steel I-shaped stub of height 500 mm making the total height of test specimen as 1570 mm. The steel stubs were then connected to the steel rails made of I-sections, which were anchored to the strong test floor (Figs. 4 and 5). It should be noted that the steel I-shaped stubs, connected to the lower part of the RC columns, were designed so that their flexural stiffness is approximately the same as that for the RC columns. Longitudinal reinforcement of beams was comprised of 4ϕ16 mm rebars on both bottom and top faces and 2 legged ϕ8 mm rebars were used as stirrups at 100 mm center-to-center spacing. The longitudinal reinforcement for columns comprised of 8ϕ16 mm rebars, and ϕ8 mm ties were provided as transverse reinforcement at variable spacing, as shown in Fig. 1. The precast beam-column connection was comprised of a corbel rebar grouted with the beam. The beam had hollow circular pockets of diameter 60 mm for the corbel rebar to pass through. Before grouting, the beam was made to rest on the corbels and a 20 mm thick neoprene pad was used to cushion the assembly. Grouting was then done using a non-shrink modified cementitious grout. Monolithic specimen MC-SMF had the same concrete dimensions and reinforcement detailing of precast

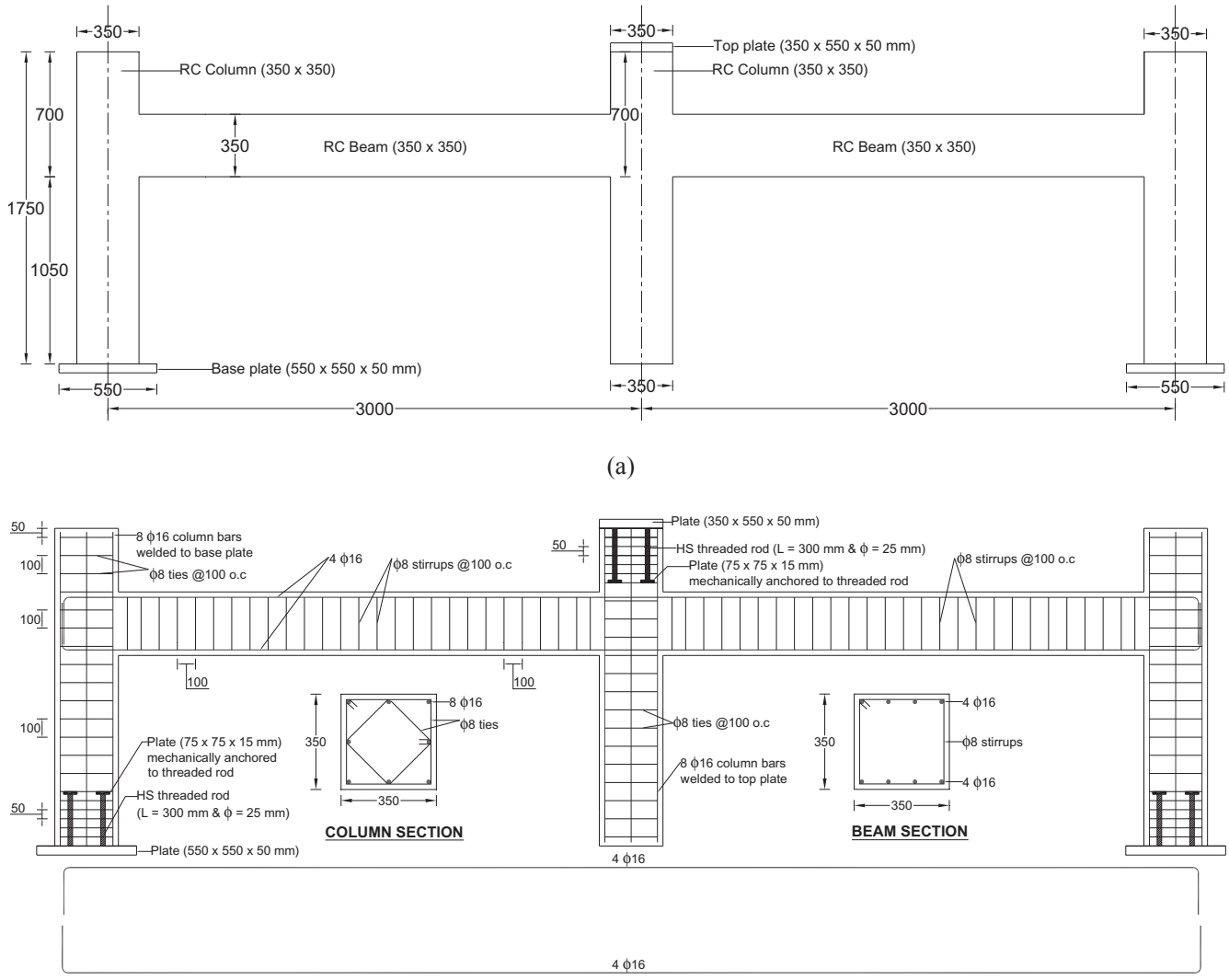

Fig. 2. Details of monolithic specimen MC-SMF (Note: All dimensions are in mm): (a) Test specimen; (b) Reinforcement details.

specimen PC-C except that it was constructed with no corbels and both top and bottom beam rebars were continuous throughout the joint regions, as shown in Fig. 2.

Steel plate strengthening scheme was designed using the nominal material properties without dynamic increase factor due to strain rate effects. The design was carried out to have flexural and shear capacity of beams of strengthened specimen PC-S approximately same as those for beams of monolithic specimen MC-SMF. The design was conducted using ASTM A572 G50 steel due to its availability in the local market. The estimated plate thickness per side was about 5.8 mm; however, the next available plate thickness in the local market was 10 mm. The selection of higher thickness was also to make up for the weak connection and to ensure sufficient margin of safety. It was thus decided to use ASTM A572 G50 steel plates with dimensions of 1050 × 350 × 10 mm and 1750 × 350 × 10 mm for exterior and interior connections, respectively. The strengthening plates were extended over a length equal to twice the beam depth measured from the face of the column toward mid-span, at both ends of the beam. This was done to cover the plastic hinge region near beam-column connection, which comes in line with the provisions of Section 21.5 of the ACI 318-11 code [36] for special RC moment frames. The connection between the steel plate and the columns and beams was designed to rely only on threaded rods, which were designed to carry the anticipated shear forces in a double-shear configuration considering limits of maximum spacing between rods (see Fig. 3). The assembly and the strengthening of precast specimen PC-S were carried out as would be followed in the field. All three columns were first erected on the column supports. The neoprene pads were then placed on corbel locations and the beam which was carried by overhead crane was then brought and slowly lowered to rest on the corbels. It was made sure that the single corbel rebar went through the beam pockets at both the ends which would be used for grouting. After PC-S specimen was assembled, the surfaces of the beam-column regions were ground manually and then sand blasting was done in order to have good bond between concrete and steel plates. The plates were bonded to the beam-column regions using a combination of epoxy adhesive mortar (Sikadur-31 produced by Sika [37]) and post-installed high strength threaded rods with 25-mm diameter and 450-mm length. Holes of 28-mm diameter were first drilled in the beam-column regions, as shown in Fig. 4(a) to accommodate the threaded rods. The holes were then cleaned using water and air compressor to remove all dust and loose particles from its inner surface. The epoxy adhesive mortar (Sikadur-31 produced by Sika [37]) was applied on the surfaces of threaded rods and the rods were subsequently inserted into the drilled holes. Care was taken to make sure that all holes were fully filled up with the adhesive material and the excess epoxy was then removed. The contact surfaces of both concrete substrate and steel plates were cleaned using acetone

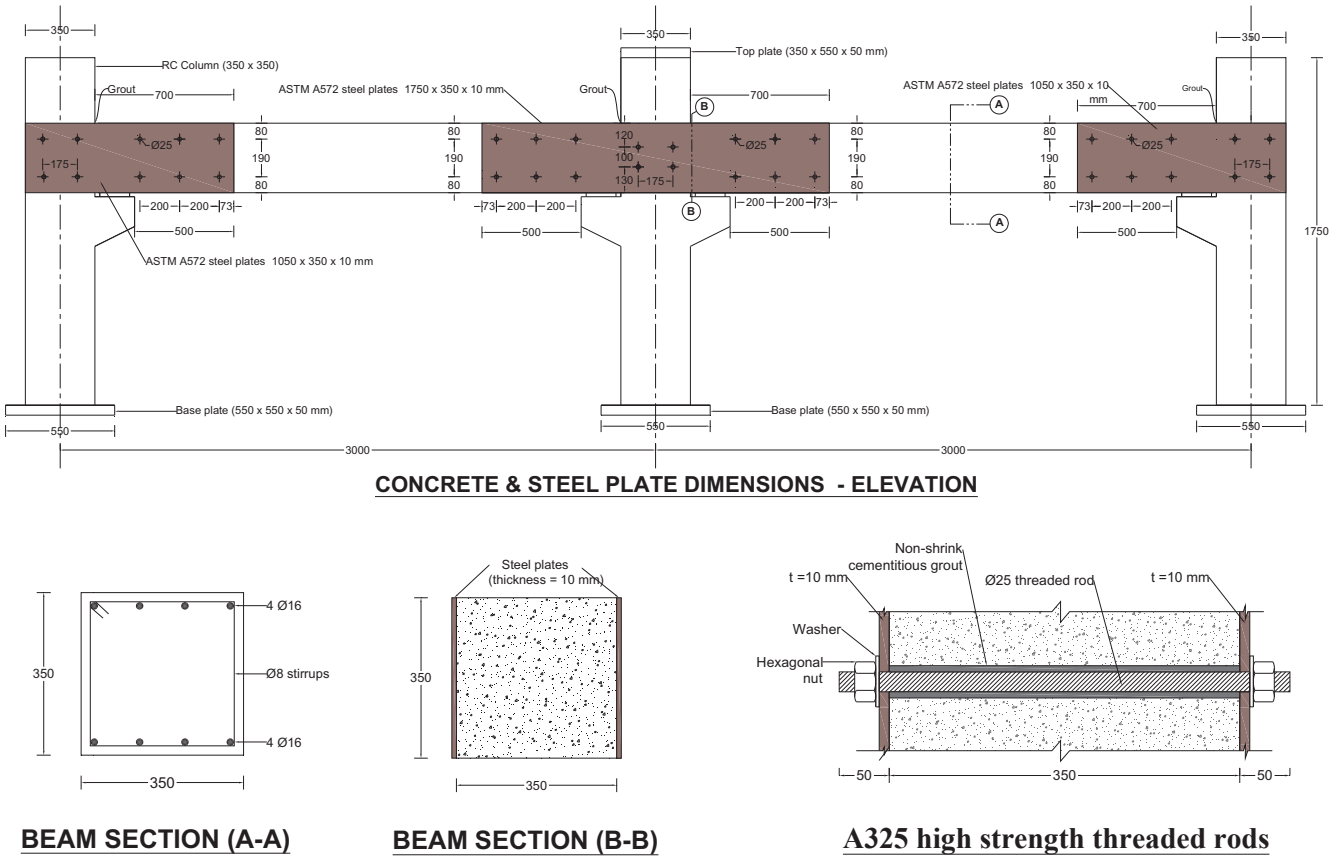

Fig. 3. Details of strengthened specimen PC-S (Note: All dimensions are in mm).

Table 1
Geometric properties of prototype frames and test specimens.

Type	Beam net span (mm)	Beam size (mm)		Column size (mm)	Corbel size (mm)	Type of connection
		Depth	Width			
Prototype	5240	700	700	700 × 700	700 × 500	Precast with grouting of corbel rebar
Specimen PC-C	2620	350	350	350 × 350	350 × 250	Precast with grouting of corbel rebar
Specimen MC-SMF	2650	350	350	350 × 350	–	Monolithic
Specimen PC-S	2620	350	350	350 × 350	350 × 250	Precast with grouting of corbel rebar

to clear any dirt, grime and loose materials from the surface. A bonding agent (Sika 31) was then applied to the concrete surface and to the surface of the steel plate in contact with the concrete. The plates were affixed in position and a pressure was applied on the plates using steel clamps. After curing of the epoxy adhesive material, the plates were tied down to the concrete surface using washers and nuts at the threaded rod locations. Attention was paid to make sure that the nuts are tied strongly to the plate so that there are no gaps between the plate and the concrete. The hollow circular pockets at the beam ends as well as gaps at beam-column interfaces were all filled with non-shrink modified cementitious grout. Fig. 4 shows the steps involved in strengthening of PC-S specimen. Fig. 5(a) shows specimen PC-S after steel plate strengthening and just before onset of testing. It should be noted that the proposed upgrading technique can be implemented in case of exterior and interior precast RC beam-column assemblies with or without floor slabs where the beams rest on corbels without transverse beams. Practical cases of non-existence of transverse beams at connection region may include circumstances where the transverse beams are not connected directly to the beam-column joint but are connected to the main beam at a certain distance from the column face, for example when there are openings in slabs or when the edge-side columns of the building are not connected directly to the transverse beams. For the cases of precast beams with dapped ends and/or transverse beams, this technique may not be constructible. It should be also noted that this strengthening scheme would be practical for cases when the column width is the same as the beam width. For the situation when the column width is larger than the beam width, premold mortar blocks might be used to cover up the difference in width and these blocks shall be well anchored to the precast beams.

2.3. Properties of materials

Ready-mix concrete was used for casting the test specimens. The specified compressive strength measured as per the ASTM C39/C39M [38] at the time of the test was 37.3 MPa (Standard deviation, SD = 2.1 MPa). For steel rebars, tensile tests were carried out in accordance with ASTM E8/E8M [39] and the average values of yield strength of ϕ8 and ϕ16 mm rebars were 525 and 526 MPa (SD = 7.2 and 8.9 MPa respectively), respectively. However, the average values of tensile strength of ϕ8 and ϕ16 mm rebars were 550 and 651 MPa (SD = 8.3 and 9.4 MPa respectively), respectively. For steel plates, standard tension test coupons were cut, machined and then tested in

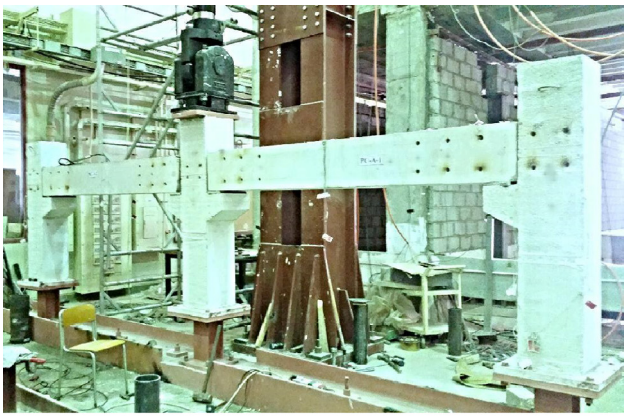

(a)

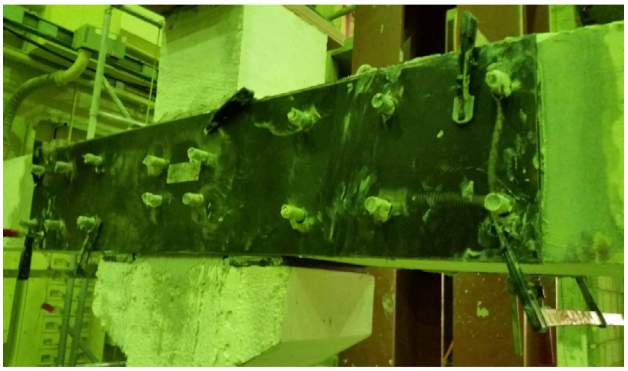

(b)

Fig. 4. Steps involved in steel plate strengthening of specimen PC-S: (a) Drilling of holes within beam-column regions; (b) Affixing of steel plates in position.

accordance with ASTM A370 - 16 [40] and the average values for yield and tensile strength of plates were 408 and 504 MPa (SD = 5.8 and 7.6 MPa respectively), respectively. The average values reported above for all materials are based on the test results of three test specimens.

2.4. Test setup and procedure

A steel loading frame shown in Fig. 5(a), which exists in the structural lab of King Saud University, was used for testing the specimens. The exposure of a building to blast loading may lead to the sudden removal of a column, which may lead to the progressive collapse of the structure. This was simulated by removing the support of the test column and exerting a dynamic load on that column using an actuator of 1000 kN capacity. The test specimen was placed in position on steel rails, which were anchored to the strong lab floor. The test column was then attached to the actuator using four high strength threaded rods of 25-mm diameter. All column bases except that of the test column were clamped to the steel rails.

A high speed data acquisition system was used to collect data at a speed of 1 k/s. The individual beam and column members of the specimens were instrumented for recording the state of stress in rebars by using strain gages affixed to the rebars. The center column and beam mid-span displacements were measured using laser transducers. Fig. 5(a) and (b) depict the complete instrumentation layout for the precast specimen PC-S.

The support underneath the test column was removed but the test frame was still in undeformed state because of the connection of test column to the actuator. This connection allows only for vertical column displacement and in-plane rotation of test specimen and restrains all other degrees of freedom. At this stage, all sensors were initialized to zero setting. The exposure of a building to blast loading may lead to the sudden removal of a column, which may lead to the progressive collapse of the structure. This was simulated by releasing the support of the middle test column and applying sudden load on that column. Since the ultimate load capacity of the specimen is not known prior to testing and in order to mimic the post-peak softening behavior of the test frame, a displacement controlled loading was adopted for the middle column. The typical target displacement-time history used for specimen testing is given in Fig. 6. A 1000-kN fatigue-rated MTS actuator was employed for load application. In real progressive collapse scenarios due to blast threats, the column is removed suddenly with very high speed (blast pressures normally yield loads associated with strain rates in the range of 100–10,000 s^{-1} [41]). However, this very high speed cannot be accommodated in the experiments due to the limits of the used actuator. The rate of loading used in this study was 100 mm/s, which is low compared with the actual scenarios. The loading rate adopted (i.e. 100 mm/s) was the maximum possible for the actuator and thus the inertial effects in experiments were of smaller scale than expected in a column-removal scenario. It is worth mentioning here that the increase in stresses due to the inertial forces is partly compensated by the enhanced material strength due to strain rate effect and moreover it is expected to have similar effect on the two types of specimen and thus the comparative performance evaluation may not be affected. The load on the test column was applied using the actuator in cycles of incremental vertical displacement in each cycle with sufficient rest period after each state of loading (Fig. 6). The increments were used to capture the behavior of specimen at different displacement levels. The rest period was utilized for taking note of the observations and marking the cracks. The unloading was done at a slow speed of 5 mm/s as it is not simulating the case of cyclic loading in seismic events. The difference between the loading protocol used herein and that used in quasi-static cyclic loading for simulating seismic actions is that in the latter, fully reversed cycles with same rates of loading and unloading are adopted. It should be noted that the loading protocol of this study (shown in Fig. 6) has been used by the authors in prior progressive collapse simulation tests on monolithic RC frames [18].

Although the number of stories of such typical buildings may vary from six to eight, the consideration of only one story is not expected to significantly alter the findings reported in this study because the large displacement response of critical members is almost unaffected by these assumptions. However, the gravity loads from upper floors are applied through the actuator. It should be also noted that axial loads were not applied on the exterior columns of the test specimens and this can be explained in the following. In case of precast specimen PC-C, axial load on exterior columns will have no effect on the capacity of test specimen as it goes directly to the exterior column support and will not affect the middle joint due to the free rotation at beam ends. For the other two specimens, ignoring axial load on exterior columns can be justified as follows:

The specimens tested in this study are scaled down from a perimeter two-bay frame of an existing building and one of the exterior columns of the test frame would represent the corner columns of the building. Corner columns are usually lightly loaded with applied factored axial loads usually less than the balanced axial load. For such a case, the flexural capacity of the column section decreases as the column axial load decreases with the worst-case scenario of minimum flexural capacity and stiffness corresponding to zero axial load. This worst-case condition was simulated in the experiments in order to reduce the flexural stiffness of the exterior columns and hence increase the deformation of the middle joint of specimens MC-SMF and PC-S.

3. Test results and discussion

Table 2 shows a summary of the test results of three specimens in terms of key parameters of load-displacement curves. It should be noted that the ultimate state used in Table 2 is defined as the state where the load drops to 80% of its peak value based on New Zealand Standard-1992 [42]. In the following sections, the test results have been

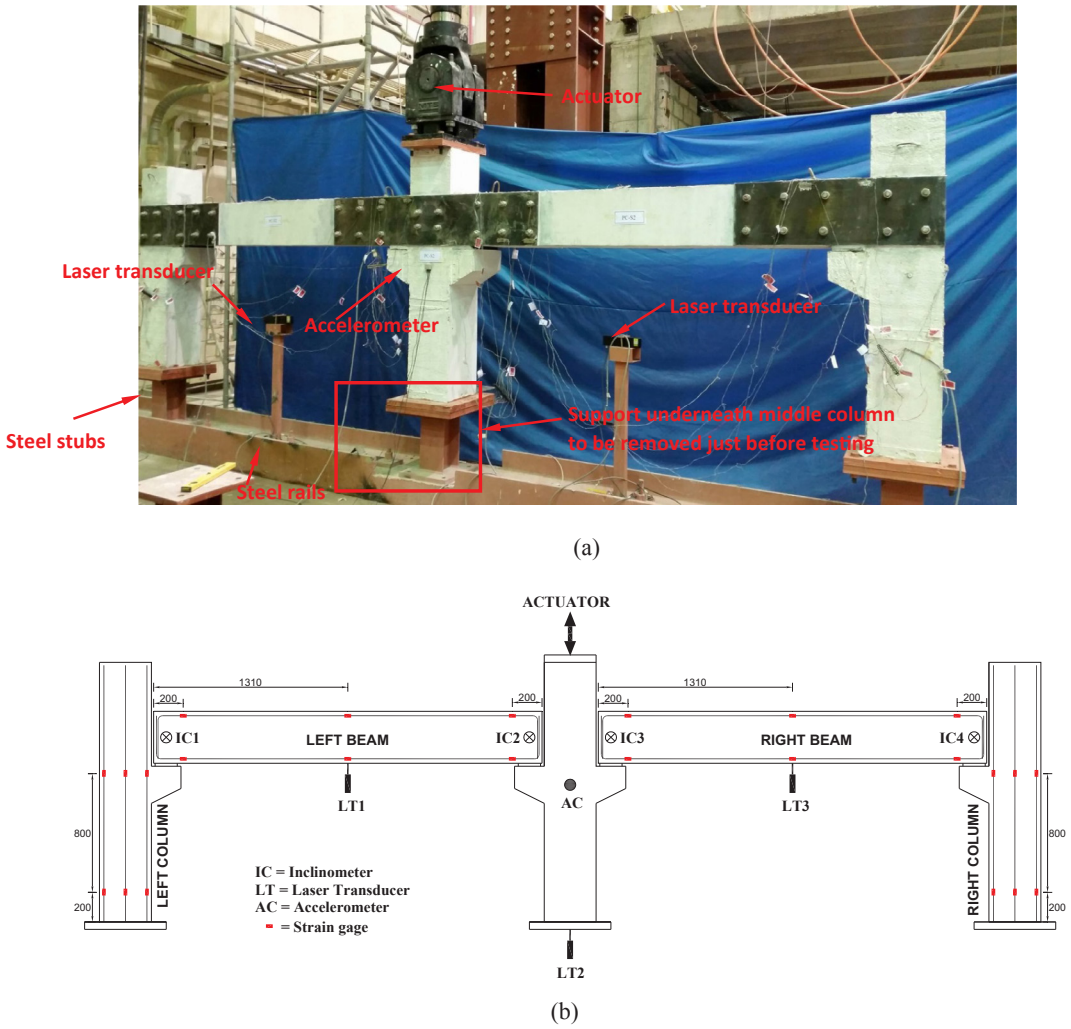

Fig. 5. Instrumented specimen PC-S: (a) Specimen ready for testing; (b) Instrumentation layout for the measurement of displacements, rotations and strains (Note: All dimensions are in mm).

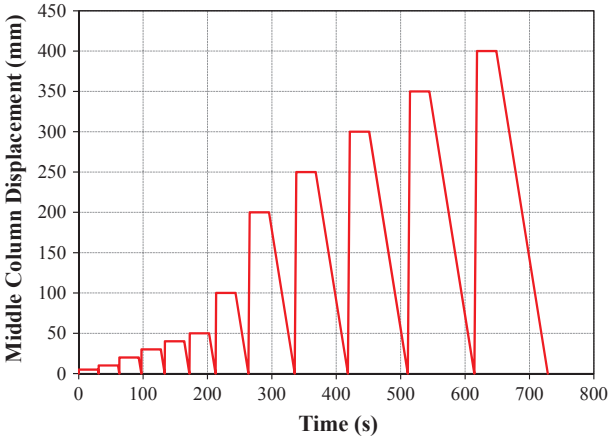

Fig. 6. Typical target displacement-time history for specimen testing.

presented in terms of mode of failure and load-displacement behavior.

3.1. Modes of failure

Final modes of failure for the three specimens are illustrated in Figs. 7 and 8. As seen in Fig. 7(a) for specimen PC-C, due to the neoprene pads the beams rotated freely at their ends, which could simulate a hinge behavior. This performance was expected due to the discontinuity of beam reinforcement at beam-column joints and hence the absence of redundancies in the load paths. During the test, both the beams of specimen PC-C were found to rotate at their ends until the interior ends came in contact with the middle column, and the ultimate mode of failure was due to concrete crushing at the location of interior beam-column connection, as seen in Fig. 7(a). Other than this, no other damage was observed in any members of specimen PC-C including beams and columns.

Fig. 7(b) depicts the final failure mode for the MC-SMF frame at the middle beam-column joint. Failure of specimen MC-SMF occurred around the middle column due to plastic hinge formation in the beam area near the connection zone. As seen in Fig. 7(b), a plastic hinge was formed near the middle joint due to large plastic strains in the bottom steel bars of the beam beyond their yield state (indicated by wide flexural cracks) accompanied with concrete crushing in the compression zone. As seen from the figure, failure of beam was not exactly symmetric on both sides of the middle column. In this case flexural action developed until the formation of plastic hinges at the middle joint. At this point, there was rapid yielding of the bottom beam rebars of the middle joint. Thereafter, yielding of the top beam rebars at the outer joints indicated the formation of the plastic hinge and that the full flexural capacity was reached. Flexural cracks were also observed in both the end columns, whereas the columns were also found to have rotated at joint locations as a result of the large deformation of the

Table 2
Experimental results for all test specimens[a].

Specimen ID	P_u (kN)	$\Delta_{u,c}$ (mm)	P_y (kN)	Δ_y (mm)	Δ_u (mm)	μ_Δ	E_u (kN·m)	$\varepsilon_{sb,bot}$ (με)	$\varepsilon_{sp,bot}$ (με)
PC-C	12.8	145	NY	NY	265	–	2.5	74	–
MC-SMF	228	144	145	25.6	269	10.5	59	95,000	–
PC-S	372	96	315	50	157	3.1	48	1300	2800

[a] P_u = peak load; $\Delta_{u,c}$ = middle column displacement at peak load; P_y and Δ_y = load and middle column displacement at first yielding of beam bottom reinforcement at inner column face; Δ_u = middle column displacement at ultimate state; μ_Δ = displacement ductility = Δ_u/Δ_y; E_u = energy dissipated at ultimate state, $\varepsilon_{sb,bot}$ = peak strain for beam bottom rebars at inner column face; $\varepsilon_{sp,bot}$ = peak strain for bottom edge of steel plates at inner column face; NY = No steel yielding.

middle column. This rotation of the columns indicated that the beam ends were not effectively restrained. Owing to this rotation, along with the limitation of actuator stroke and the discontinuity of beam members beyond the end columns, there was no development of the catenary action. As a result there was no further increase in load-carrying capacity of the frame.

Fig. 8 presents the final deformed shape and failure modes for PC-S specimen. During the displacement controlled loading stages, significant flexure-shear cracks appeared in the specimen almost symmetrically on both faces of the unstrengthened portion of beams, as seen in Fig. 8(a). The cracks in concrete were initiated in flexure mode and then propagated diagonally in shear mode towards the ends of steel plate (Fig. 8(a)). This may be attributed to combined flexure-shear stresses in the unstrengthened portion of beams. At about 50 mm vertical displacement of test column, excessive flexure-shear cracks were seen in the unstrengthened part of the right beam. Finally, at a load of 372 kN, the right beam of the test specimen failed suddenly by shear at a middle column displacement of 96 mm. The reason is that adding steel plates in the beam-column regions led to significant increase in both flexure and shear capacity of the beams at zones of beam-column connections and the load corresponding to shear capacity of the unstrengthened part of the beam was considerably less than that corresponding to flexural capacity of the strengthened portion. It is worth mentioning here that the failure occurred in the unstrengthened part of the beam and there was no connection failure. Fig. 8(c) shows a close-up view of brittle shear failure of the right beam. As seen from the figure, shear failure occurred at approximately 45° angle from the beam axis and it was accompanied by fracture of steel stirrups passing through the shear failure plane.

3.2. Load-displacement characteristics

Load versus middle column displacement hysteresis and envelopes are presented in Fig. 9 for all test specimens. Comparison of load-displacement envelopes for test frames is shown in Fig. 10. Fig. 9(a) reveals that existing precast concrete buildings are very vulnerable to progressive collapse once the supporting column is lost in an extreme event. The peak load of specimen PC-C was 12.8 kN. For monolithic specimen MC-SMF, as seen in Fig. 9(b), the load-displacement envelope can be divided into four stages. The AB segment can be considered as the elastic stage, during which the relationship between the load and the vertical displacement of middle column is linear, without obvious

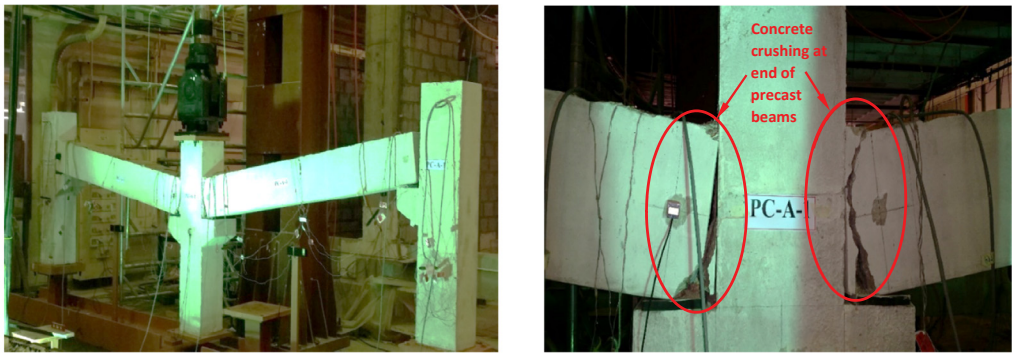

Final deformed shape *Failure of middle joint*

(a)

Final deformed shape *Failure of middle joint*

(b)

Fig. 7. Mode of failure for: (a) Specimen PC-C; (b) Specimen MC-SMF.

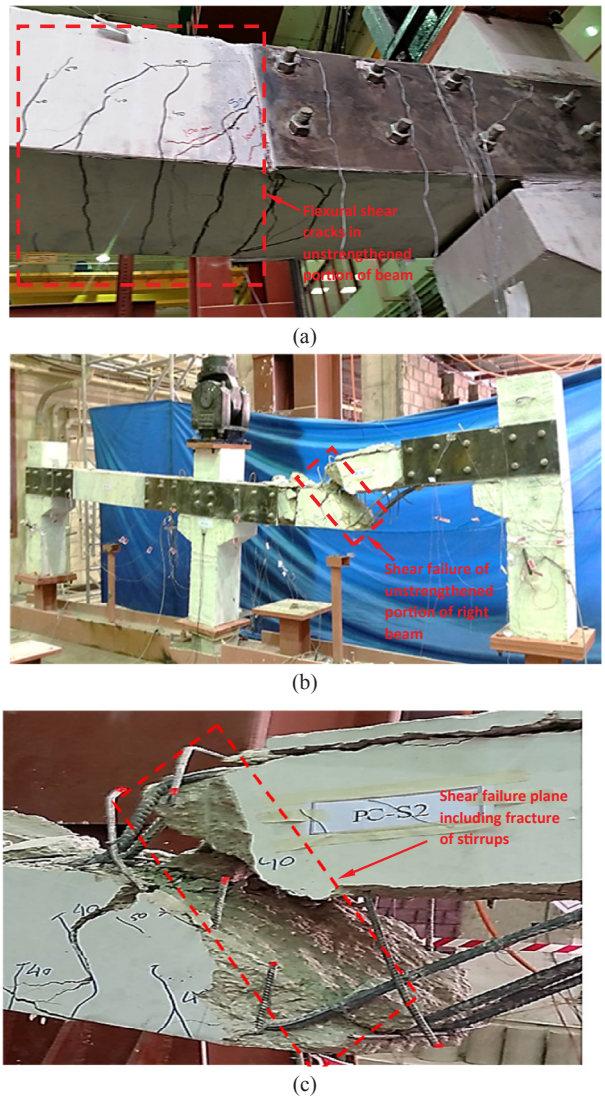

Fig. 8. Mode of failure for strengthened specimen PC-S: (a) Flexure-shear cracking in beams; (b) Final deformed shape; (c) Close-up of beam shear failure.

destruction in the frame specimen. The BC segment is the start of the inelastic stage. The load is in a nonlinear relationship with the increase of displacement and the secant stiffness begins to drop at this stage. From the recorded steel strains, it was noticed that the longitudinal rebars at the ends of beams started to yield, indicating the formation of plastic hinges in the beams. And, most of the rebars at the ends of beams had yielded at Point C. The CD segment is the plastic hinge stage. Plastic hinges at the ends of beams were formed and the frame gradually turned into a plastic stress system. Concrete crushing was observed from Point C and concrete spalling appeared at a later period in this stage. The progressive collapse resistance of the test frame began to decrease after reaching a middle column displacement of about 250 mm, as shown in Fig. 9(b). The DE segment is the catenary action stage. The flexural capacity of beams was almost lost at this stage. At the inner beam-column connection, the flexural tension cracks penetrated through the compression zones, indicating the formation of the catenary mechanism at the inner joint. However, because the outer beam-column joints were unable to provide enough anchorage for the longitudinal rebars in the beams, the bearing capacity of the frame at the catenary action stage decreased continuously with the increment of the vertical displacement. The structure entered an irreversible collapse process and the test was terminated due to the limitation of the actuator stroke (at Point E). From the load-displacement comparison presented

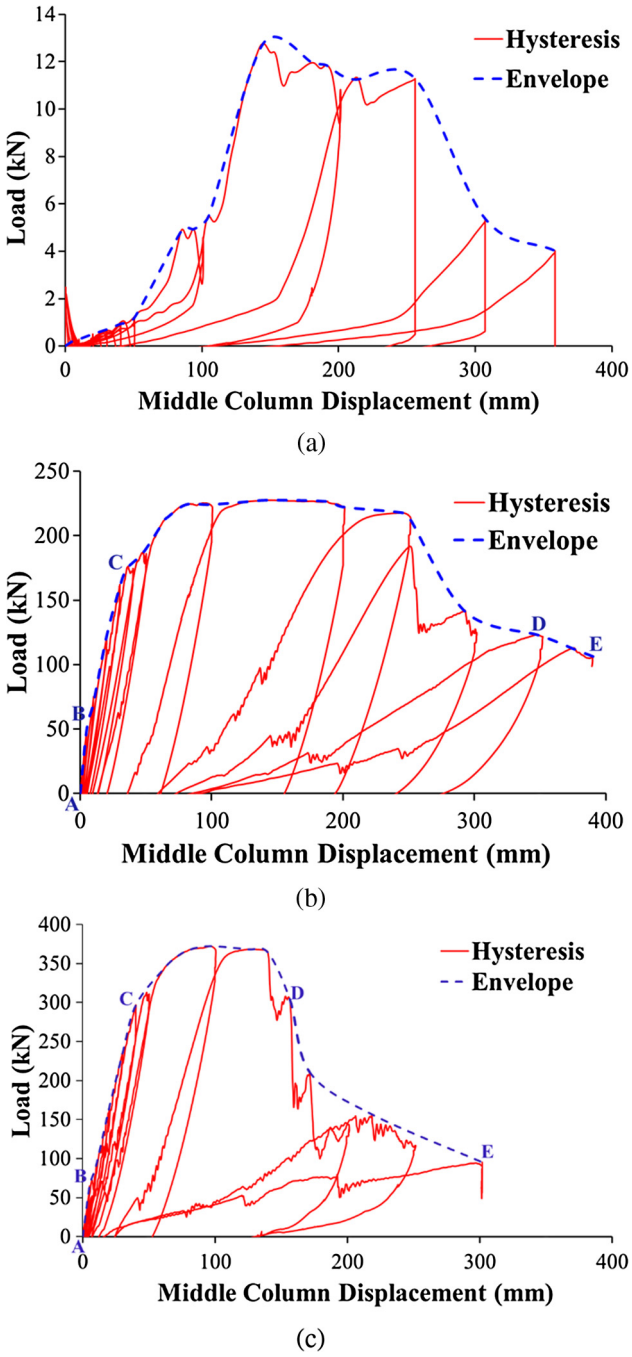

Fig. 9. Load-displacement hysteresis for: (a) Specimen PC-C; (b) Specimen MC-SMF; (c) Specimen PC-S.

in Fig. 10, it is clear that the monolithic specimen MC-SMF has excellent performance compared with the precast control specimen PC-C. The peak load resisted by specimen MC-SMF was 228 kN which is about 17.8 times of that for specimen PC-C. In addition, and as depicted from Table 2, energy dissipated at ultimate state of specimen MC-SMF was very high as compared to precast control specimen PC-C. The excellent performance of the monolithic specimen MC-SMF was expected due to the continuity of the beam rebars and hence the redundancies in the load paths.

For strengthened specimen PC-S, as seen in Fig. 9(c), the load-displacement envelope can be divided into four stages. The AB segment can be considered as the elastic stage. The BC segment is the onset of the inelastic stage. From the recorded steel plate strains, it was noticed that the bottom edge of steel plates at inner column face had already

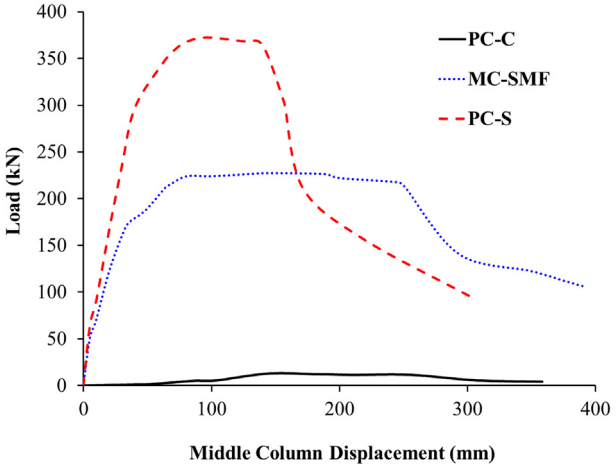

Fig. 10. Load-displacement envelope comparison for test specimens.

yielded at point C; however, top edge of steel plates at outer column faces did not reach their yield strain at point C. The CD segment is the flexure-shear cracking stage in the right beam. During this stage, flexure-shear cracks started in the unstrengthened part of the right beam. The peak load of the specimen was recorded during this stage at which shear failure associated with fracture of steel stirrups occurred in the unstrengthened portion of the right beam. Due to brittle shear failure in the CD segment, there is no catenary action in the DE segment. It is clear that strengthened specimen PC-S had considerably higher load as compared to other two control specimens. The peak load resisted by specimen PC-S was 372 kN which is about 29 and 1.6 times of that for specimens PC-C and MC-SMF, respectively. In addition, and as depicted from Table 2, energy dissipated in specimen PC-S was significantly higher than that for control precast specimen PC-C (about 19 times). However, displacement ductility ratio and energy dissipated in strengthened specimen PC-S were about 30% and 82%, respectively, of those for control monolithic specimen MC-SMF. In conclusion, strengthening of precast RC beam-column connections using bolted steel plates was found efficient in increasing the peak load of specimen under column-removal scenario. This strengthening technique increased the load significantly to about 29 times of that for specimen PC-C. Also, energy dissipated at ultimate state got increased due to steel plate strengthening. However, the drawback of this technique is that it increased the flexural capacity of the beam significantly so that it exceeded the shear capacity of its unstrengthened part and hence induced brittle shear failure. This could have been alleviated by using thinner plates.

3.3. Strain gage results

Figs. 11 and 12 show the experimental values of maximum tensile steel strains for specimens MC-SMF and PC-S, respectively. Table 2 displays peak strain for beam bottom rebars at inner column face for three test specimens. As presented in Table 2, peak strain for beam bottom rebars at inner column face of both precast specimens PC-C and PC-S were significantly lower than the rebar yield strain. This was due to the discontinuity of beam bottom rebars at the connection zone. However, for monolithic specimen MC-SMF and as presented in Fig. 11 and Table 2, all tension rebars (at the ends of beams and at outer columns near connection zone) had yielded and large tensile strains were noted, thereby indicating plastic hinge formation at the ends of beams, as previously outlined. For strengthened specimen PC-S and as seen in Table 2 and Fig. 12, tensile strain of about 1.4 times the yield strain was noted at the bottom edge of steel plate at inner column face; however, the top edge of steel plate at outer column face did not reach the yield strain. This reveals that neither of the steel-plated sections of beams of

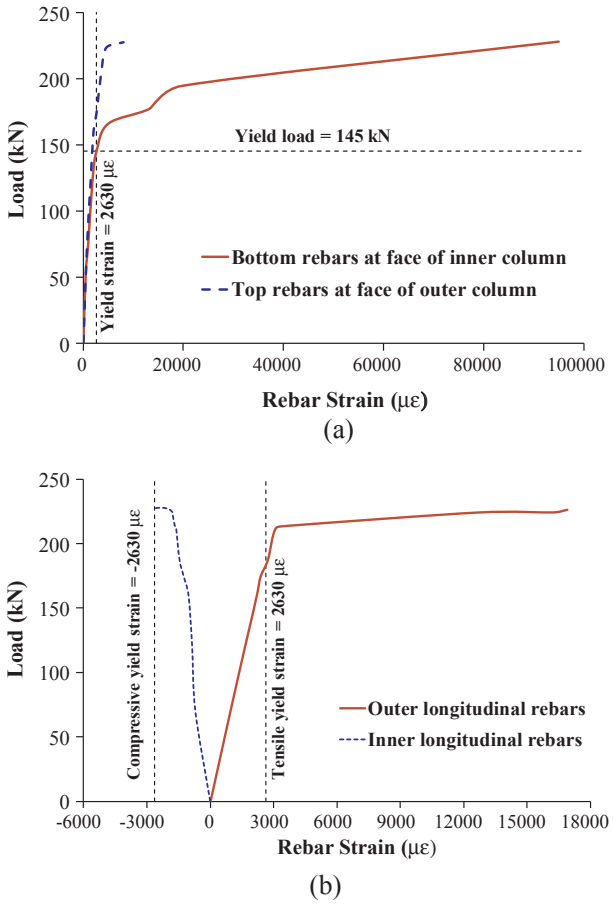

Fig. 11. Load versus rebar strain curves for specimen MC-SMF: (a) Longitudinal beam rebars at column face; (b) Longitudinal column rebars near connection zone.

specimen PC-S reached its ultimate flexural capacity due to brittle shear failure of the unstrengthened part, as discussed previously. However, due to the high ultimate load resisted by specimen PC-S, its exterior columns reached their flexural capacity at the end of test by having large tensile strains of about 20,000 με for outer rebars, as seen in Fig. 12(b).

4. Analytical modeling

Simplified section analysis procedure was followed in order to compute the ultimate capacity of specimens MC-SMF and PC-S. Theoretical peak loads were then compared with the experimental values. As the experiments involved testing of specimens at a loading rate of 100 mm/s, the first step in the analysis is to estimate the dynamic increase factor (*DIF*) of the constituent materials due to strain rate effects. The equation of the CEB-FIP Model Code 90 [43] of strain rate effect was used to assess the *DIF* for the concrete compressive strength using the following equations:

$$\frac{f'_{cd}}{f'_{cs}} = DIF = \begin{cases} \left(\frac{\dot{\varepsilon}}{\dot{\varepsilon}_s}\right)^{1.026\alpha} & \text{for } \dot{\varepsilon} \leqslant 30\ \text{s}^{-1} \\ \gamma\left(\frac{\dot{\varepsilon}}{\dot{\varepsilon}_s}\right)^{1/3} & \text{for } \dot{\varepsilon} > 30\ \text{s}^{-1} \end{cases} \quad (1)$$

where f'_{cd} = compressive strength of concrete with strain rate effect included; f'_{cs} = static compressive strength of concrete; $\dot{\varepsilon}$ = strain rate; $\dot{\varepsilon}_s$ = quasi-static strain rate = $30 \times 10^{-6}\ \text{s}^{-1}$ and α is a factor given by

$$\alpha = \frac{1}{5 + 0.9f'_{cs}} \quad (\text{units of } f'_{cs}\text{: MPa}) \quad (2)$$

The parameter γ in Eq. (1) is estimated from

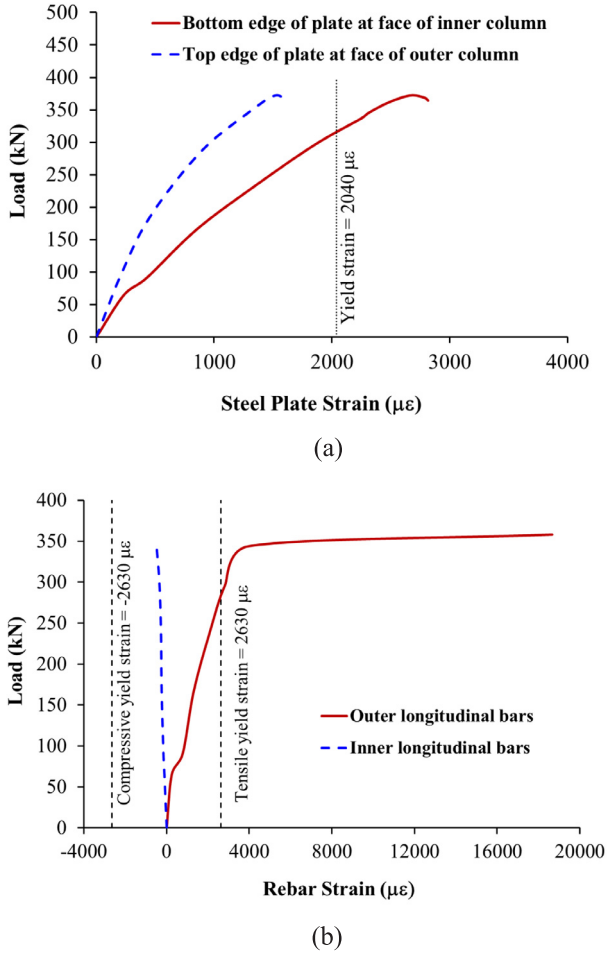

Fig. 12. Load versus steel strain curves for specimen PC-S: (a) Edge of steel plate at column face; (b) Longitudinal column rebars near connection zone.

$$\log\gamma = 6.156\alpha - 2 \tag{3}$$

For steel rebars and plate, the model proposed by Malvar [44] was utilized to compute the *DIF* for both yield and ultimate strength as follows:

$$DIF = \left(\frac{\dot{\varepsilon}}{10^{-4}}\right)^{\alpha_s} \quad (\text{units of } \dot{\varepsilon}\text{: } s^{-1}) \tag{4}$$

where for calculating yield strength, $\alpha_s = \alpha_{fy}$, which is estimated from

$$\alpha_{fy} = 0.074 - 0.04\frac{f_{ys}}{414} \quad (\text{units of } f_{ys}\text{: MPa}) \tag{5}$$

However, for calculating ultimate strength, $\alpha_s = \alpha_{fu}$, and is given by

$$\alpha_{fu} = 0.019 - 0.009\frac{f_{ys}}{414} \quad (\text{units of } f_{ys}\text{: MPa}) \tag{6}$$

where f_{ys} = static yield strength of steel rebars (or plate) in MPa units. It should be noted that the strain rate used to calculate *DIF* in Eqs. (1) and (4) was taken as $0.01\ s^{-1}$. This value was obtained from the experimental testing of the three specimens detailed previously as an average value based on strain versus time recordings. The ultimate capacity was then computed as follows:

4.1. Specimen MC-SMF

4.1.1. Based on flexural capacity of beams

Internal strain and stress distribution for beam section of specimen MC-SMF is illustrated in Fig. 13. The area of compression reinforcement is referred to as A_s', the depth to the centroid of the compression reinforcement from the extreme compression fiber of the section is d', the strain in the compression reinforcement is ε_s', the stress in the compression reinforcement is f_s', the area of tension rebars is referred to as A_s, the effective depth to centroid of tension rebars is termed as d, the strain in the tension reinforcement is ε_s and its corresponding stress is f_s. A linear strain distribution is assumed as shown in Fig. 13, and for the evaluation of the moment capacity, the compression strain in the extreme concrete compression fiber is set equal to the maximum usable concrete compressive strain of $\varepsilon_{cu} = 0.003$ [45]. The strain in the tension rebars is not known, and thus, the depth to the neutral axis, c, is also unknown. An iterative procedure was used to come up with the neutral axis depth value. A reasonable initial estimate of c was taken as $0.2d$. The value of c was adjusted after checking equilibrium. The strains in both tension and compression rebars were then calculated using similar triangles as shown in Fig. 13. The corresponding stresses were calculated from Fig. 14, assuming a bilinear stress-strain relationship for steel rebars. Tension and compression forces of steel rebars were then estimated as $T = A_s \times f_s$ and $C_s = A_s' \times f_s'$. Thus, establishing section equilibrium resulted in the following equation.

$$T = C_c + C_s \Rightarrow A_s f_s = 0.85 f_{cd}' \beta_1 cb + A_s' f_s' \tag{7}$$

where β_1 was calculated as per the ACI 318-14 code [45]. The neutral axis depth was then recalculated from

$$c = \frac{A_s f_s - A_s' f_s'}{0.85 f_{cd}' \beta_1 b} \tag{8}$$

The previous steps were repeated until convergence occurred and section equilibrium was established. The flexural capacity of the beam

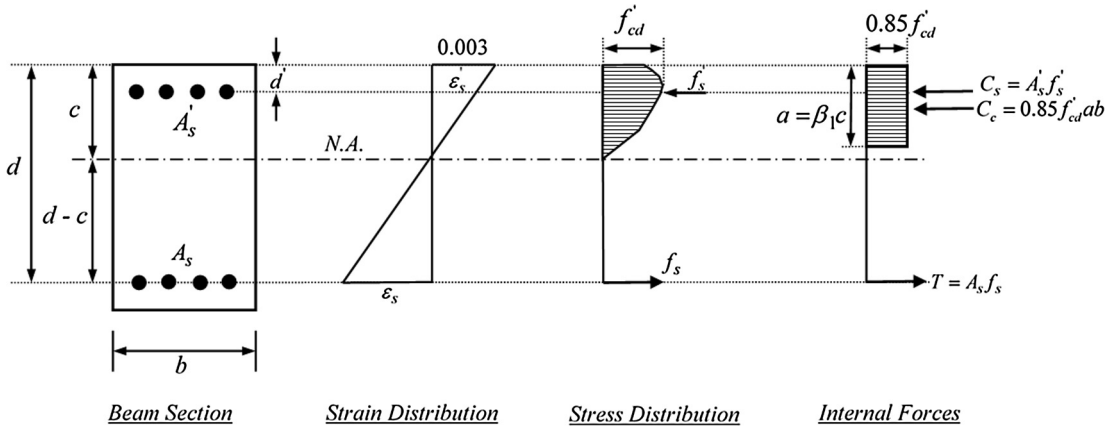

Fig. 13. Internal strain and stress distribution for beam section of specimen MC-SMF.

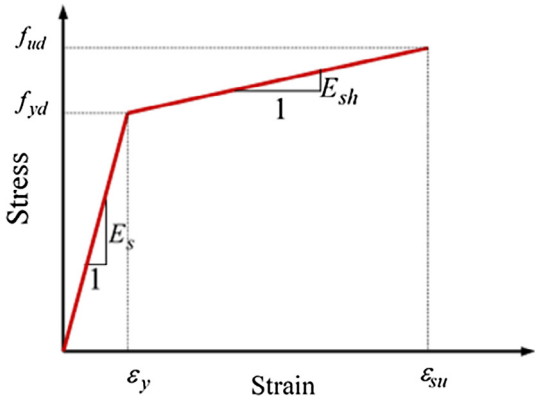

Fig. 14. Bilinear stress-strain relationship of steel rebars used for section analysis.

section was then estimated from

$$M_u = 0.85f'_{cd}\beta_1 cb\left(d-\frac{\beta_1 c}{2}\right) + A'_s f'_s (d-d') \tag{9}$$

The test frame was modeled using SAP2000 software [46] as shown in Fig. 15. Three-dimensional, two-node frame elements with 6 degrees of freedom per node were used to model beams and columns. To account for the presence of cracked regions along the length of the member, stiffness modifiers as per the ACI 318-11 code [36] were input in the model. The 500 mm height I-shaped steel stubs were also included in the model at the bottom end of the exterior columns. The bases of the exterior columns were fully restrained against displacement and rotation in the global X, Y and Z directions. A unit load was applied on the center column and the bending moment and shear force diagrams were then obtained as presented in Fig. 15(b) and (c), respectively. At the interior beam-column face, the moment was calculated from the SAP2000 model to be about 0.7 kN m. Hence, the ultimate load of the test specimen that corresponds to flexural failure of beam was estimated from

$$P_{u,f} = \frac{M_u}{0.7} \quad \text{(units: kN and m)} \tag{10}$$

4.1.2. Based on shear capacity of beams

The shear capacity of beams was estimated from the following additive equation:

$$V_u = V_c + V_s \tag{11}$$

where V_c = concrete shear strength contribution and V_S = shear resisted by stirrups. Since beams of test frames underwent large deformation associated with both wide flexure cracking extending into the neutral axis and concrete crushing in the compression zone, concrete contribution to shear strength should be reduced [47,48]. The model adopted by Priestley et al. [47] and Elsanadedy and Haroun [48] was used. In this model, concrete component is expressed as

$$V_c = 0.05\lambda_1\lambda_2\sqrt{f'_{cd}}\,b(d-c) \quad \text{(units: N and mm)} \tag{12}$$

where λ_1 is a factor that accounts for aspect ratio of element and is conservatively assumed as 1.0 and λ_2 is a factor that considers the effect of tension steel ratio and is given as $\lambda_2 = 0.5 + 20\rho_s$, where ρ_s = tension steel ratio of beam = A_s/bd. It should be noted that the above model of Eq. (12) was developed for plastic hinge region of columns under seismic actions in which concrete degrades severely due to seismic loading. This model was adopted in this study as the behavior of concrete in the beams near middle column is similar to plastic hinge zones of columns under earthquake events in terms of large and wide cracking in the tension side associated with crushing in the compression side. According to Priestley et al. [47] and Elsanadedy and Haroun [48], the shear strength resisted by stirrups may be estimated from

$$V_s = \frac{A_v f_{yhd}(d-c)}{s} \tag{13}$$

where A_v = area of shear reinforcement, f_{yhd} = yield strength of stirrups amplified due to strain rate effect as discussed previously, and s = center-to-center spacing between stirrups. The aforementioned procedure was followed to compute the shear strength of beam section near connection zone. As per the shear force diagram shown in Fig. 15(c), the ultimate load of the test specimen corresponding to shear failure of beams was calculated from

$$P_{u,sh} = \frac{V_u}{0.5} \tag{14}$$

4.1.3. Based on shear friction at beam-column interface

The model adopted by the ACI 318-14 code [45] was used to compute the strength corresponding to direct shear transmitted at beam-column interface from the following formula:

$$V_{u,SF} = \mu A_{vf} f_{yd} \leqslant \begin{cases} 0.2f'_{cd}A_c \\ (3.3 + 0.08f'_{cd})A_c \\ 11A_c \end{cases} \quad \text{(units: N and mm)} \tag{15}$$

where A_{vf} = area of shear friction reinforcement = $A_s + A'_s$; f_{yd} = yield strength of longitudinal beam reinforcement, increased due to strain rate effect; μ = coefficient of friction at shear transfer plane = 1.4 in case of monolithically cast concrete such as specimen MC-SMF; and A_c = area of concrete section resisting shear transfer = bd. The ultimate load based on shear friction at beam-column interface was then estimated from

$$P_{u,SF} = \frac{V_{u,SF}}{0.5} \tag{16}$$

The final ultimate load of specimen MC-SMF was then taken as the least of that given by Eqs. (10), (14) and (16).

4.2. Strengthened specimen PC-S

4.2.1. Based on flexural capacity of strengthened portion of beams

Fig. 16 shows internal strain and stress distribution for beam section of specimen PC-S at ultimate state. The steel plate section was first divided into thin slices. Number of steel plate slices (n) was assumed as 20 and the height of each slice was taken as $h_s = 0.05\,h$. The effective depth of the i^{th} slice was then estimated as $d_{si} = h-(i-1)h_s-0.5h_s$. As mentioned previously, epoxy adhesive mortar was used as a bonding agent at the steel plate-to-concrete interface, which could prohibit the unwanted interfacial plate debonding. However, due to the insufficiency of the threaded rods at the beam-column interface, concrete cover delamination may occur and the plate could separate from the beam with some part of concrete cover attached to it. Although buckling was not observed in the experiments due to the overdesign of the steel plates, the thinner plates may be susceptible to out-of-plane buckling in the compression zone. Therefore, steel plate contribution in compression was ignored and stresses in its slices of the compression zone were set equal to zero. A reasonable initial estimate of c was taken as $0.2\,h$. The value of c was adjusted after checking equilibrium. Using similar triangles, as seen in Fig. 16, the strain value at the center of the i^{th} slice was calculated from

$$\varepsilon_{si} = 0.003\left(\frac{d_{si}-c}{c}\right) \tag{17}$$

Assuming a bilinear stress-strain relationship for steel plates as that seen in Fig. 14, the stresses in the i^{th} slice was computed. The internal force of the i^{th} slice was calculated as $F_{si} = A_{si}f_{si} = 2t_p h_s f_{si}$, where t_p = thickness of steel plate. The neutral axis depth was then recalculated from

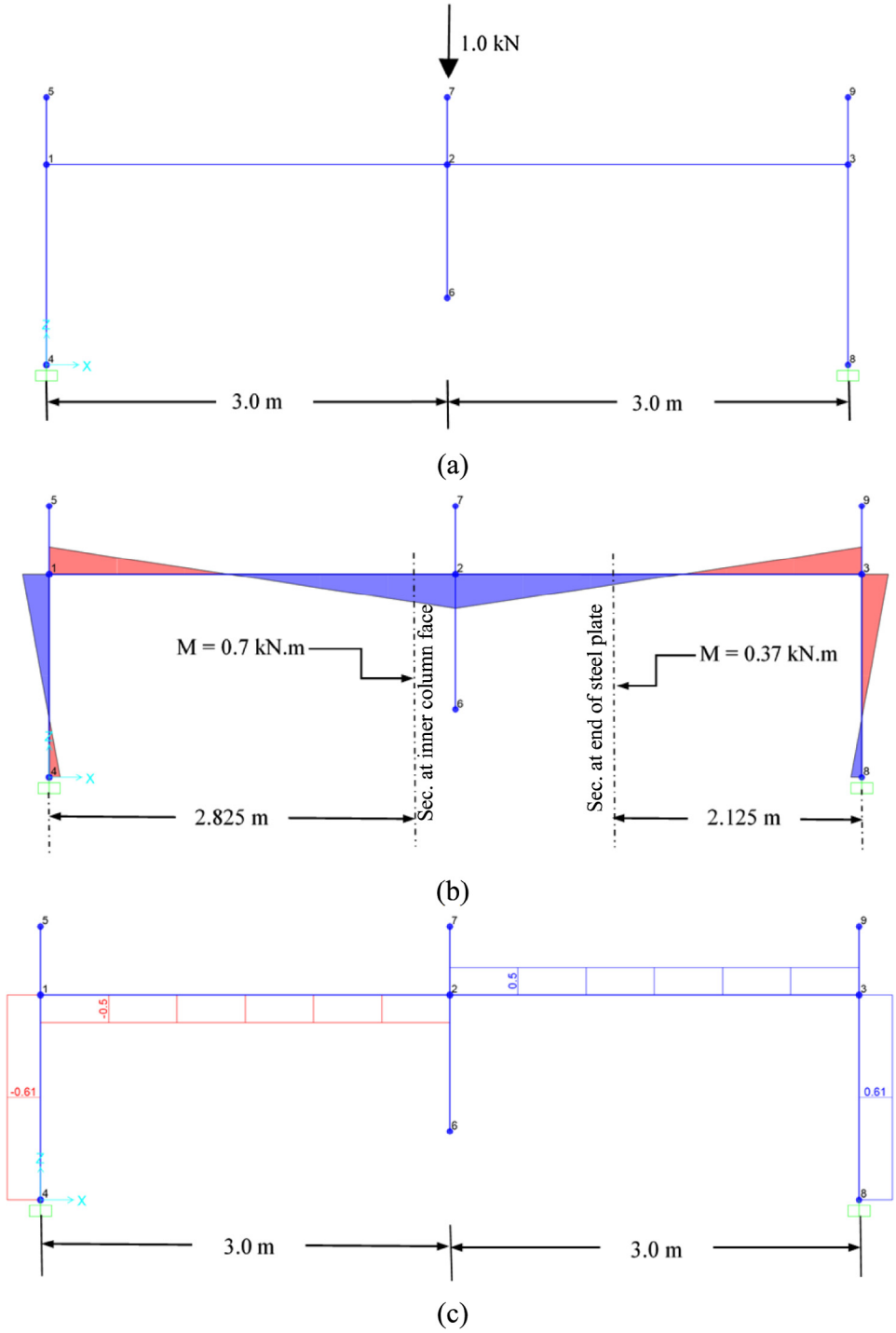

Fig. 15. Linear elastic frame analysis of specimens MC-SMF and PC-S using SAP2000: (a) Unit vertical load at middle column; (b) Bending moment diagram for the frame due to unit load; (c) Shear force diagram for the frame due to unit load.

$$c = \frac{\sum_{i=1}^{n} F_{si}}{0.85\beta_1 f'_{cd} b} \tag{18}$$

The previous steps were repeated until convergence occurred and section equilibrium was established. The flexural capacity of the beam section was then estimated from

$$M_u = \sum_{i=1}^{n} F_{si}\left(d_{si} - \frac{\beta_1 c}{2}\right) \tag{19}$$

Hence, the ultimate load of the test specimen that corresponds to flexural failure of strengthened portion of beams was estimated from Eq. (10).

4.2.2. Based on shear capacity of strengthened portion of beams

Since beams of test frames underwent large displacement associated with wide flexure cracking and concrete crushing in the compression zone, concrete contribution to shear strength was ignored in assessing shear strength of strengthened part of beams. This was done similar to plastic hinge zones of columns under seismic actions as they have the same behavior of large and wide cracking in the tension side associated with crushing in the compression side [48]. The shear capacity was

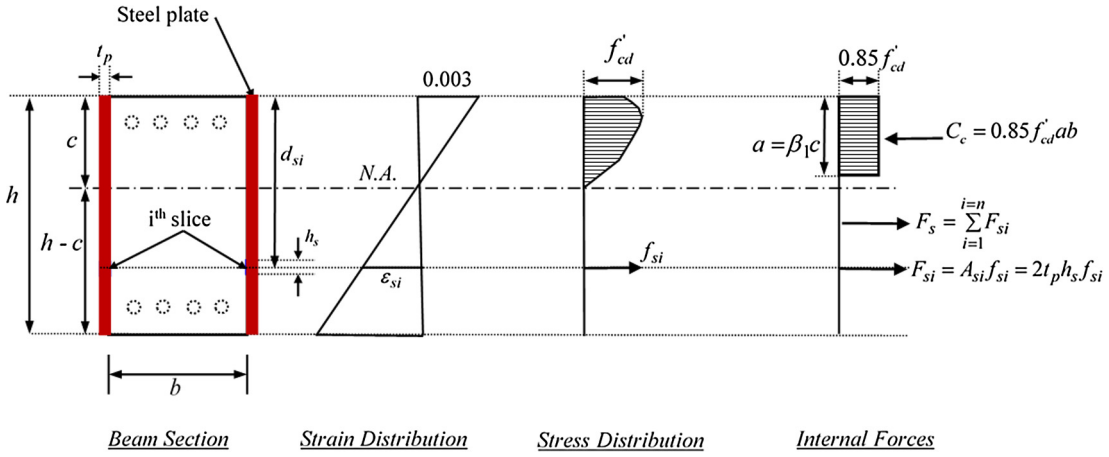

Fig. 16. Internal strain and stress distribution for beam section of specimen PC-S.

then assumed as $V_u = V_p$, where V_p is the shear carried by steel plates, calculated using the following formula proposed by Elsanadedy and Haroun [48].

$$V_p = 2t_p f_{ypd}(h-c) \tag{20}$$

The ultimate load of the test specimen corresponding to shear failure of strengthened part of beams was calculated from Eq. (14).

4.2.3. Based on shear friction at beam-column interface

As per the ACI 318-14 code [45], the direct shear transmitted at beam-column interface was estimated from

$$V_{u,SF} = \mu A_{vp} f_{ypd} \leqslant \begin{cases} 0.2 f'_{cd} A_c \\ 5.5 A_c \end{cases} \quad \text{(units: N and mm)} \tag{21}$$

where μ = coefficient of friction = 0.6 and A_{vp} = total area of steel plates passing through the beam-column interface = $2t_p h$; and A_c = area of concrete section resisting shear transfer = bh. The ultimate load based on shear friction at beam-column interface was then estimated using Eq. (16).

4.2.4. Based on capacity of unstrengthened portion of beams

Flexural capacity of unstrengthened part of beams was calculated as similar to specimen MC-SMF (Eqs. (7)–(9)). However, as seen in Fig. 15(b), bending moment at critical section of unstrengthened part of beam (end of steel plate section) due to unit vertical load at top of center column was 0.37 kN·m. Hence, the peak load that corresponded to flexural capacity of unstrengthened beam section was computed from

$$P_{u,f} = \frac{M_u}{0.37} \quad \text{(units: kN and m)} \tag{22}$$

The shear capacity of the unstrengthened portion of beam was the same as that calculated previously for beams of monolithic specimen MC-SMF (Eqs. (11)–(13)) and the corresponding peak load was estimated using Eq. (14).

The final peak load of strengthened specimen PC-S was then taken as the least of that given by abovementioned modes for strengthened and unstrengthened parts of beams. Table 3 summarizes the peak loads of specimens MC-SMF and PC-S calculated based on different possible modes detailed previously, in addition to experimental and final theoretical peak load. Illustrated in Table 3 is also the tested-to-predicted peak load ratio for the two specimens. As seen from Table 3, deviation of 4–12% is observed in the theoretical prediction of peak loads.

It is worth mentioning here that the simple linear elastic analysis of the tested frames, adopted in this section, may not be reliable for the simulation of the failure involving complex nonlinearity and large displacement. However, the adopted procedure of analysis is thought to be enough for the prediction of peak load of flexural action stage at which the displacements are not large and the employment of linear elastic analysis may be reasonable as small displacement theory may apply. However, for other action stages (such as compressive arch and catenary actions), large displacements associated with them will significantly change the position and orientation of the loads and hence, using linear elastic method of analysis will be invalid and may induce erroneous results. It is to be noted here that the compressive arch and catenary actions were not observed in the experiments.

5. Conclusions

The main findings of this study can be summarized as follows:

- Existing type of precast RC beam-column connection (grouting of corbel rebar with beam resting on corbel via neoprene pad), tested in this study, was found to have a very high potential of progressive collapse due to negligible ductility and lack of continuity in beam-column joints and hence the absence of redundancies in the load paths.
- Even though the monolithic specimen MC-SMF with continuous top and bottom beam rebars had significantly higher ultimate load and energy dissipated compared to existing precast specimen PC-C, the development of catenary action was inhibited due to limitations of

Table 3
Experimental vs. theoretical peak load for specimens MC-SMF and PC-S.

Specimen ID	Peak load based on strengthened portion of beam (kN)			Peak load based on unstrengthened portion of beam (kN)			Theoretical peak load, $P_{u,ana}$ (kN)	Experimental peak load, $P_{u,exp}$ (kN)	$\frac{P_{u,exp}}{P_{u,ana}}$
	Based on flexural capacity	Based on shear capacity	Based on shear friction	Based on flexural capacity	Based on shear capacity	Based on shear friction			
MC-SMF	–	–	–	204	360	1491	204	228	1.12
PC-S	437	3907	1348	386	360	1491	360	372	1.04

the test setup. These limitations may include: (i) absence of axial load application on exterior columns (axial load would increase the flexural stiffness of the exterior columns and then favor the development of arch and catenary action); (ii) discontinuity of beams beyond the exterior columns; and (iii) exclusion of RC floor slabs from the test specimen (presence of concrete slabs may help in the development of both arch and catenary mechanisms).

- Strengthening of precast RC beam-column connections using bolted steel plates was found effective in increasing the collapse load of assembly under column-loss scenario. This strengthening technique increased the load considerably to about 29 times of that for control precast specimen PC-C. Also, energy dissipated at ultimate state got significantly increased due to steel plate strengthening. However, it increased the flexural capacity of the beam significantly so that it exceeded the shear capacity of its unstrengthened part and hence induced brittle shear failure.
- The section analysis procedure that accounts for strain compatibility, material nonlinearity, strain rate effect and different failure modes was found appropriate in estimating the collapse load of both monolithic and steel-plated precast RC beam-column assemblies under column-removal scenario.
- In designing of steel plate strengthening scheme for provision of continuity at precast RC beam-column connections, it is recommended to extend the plates to at least twice the beam depth beyond the column face to cover the plastic hinge region near beam-column connection and to allow for full utilization of the plate strength.
- The simple linear elastic analysis of the tested frames, adopted in the study, may not be appropriate for the simulation of the failure involving complex nonlinearity and large displacement. For the prediction of peak load of actions involving large displacement (such as compressive arch or catenary actions) or full load-displacement history of the assembly, nonlinear finite element modeling will be required.

Acknowledgments

This work is based on the Project funded by the National Plan for Science, Technology and Innovation (MAARIFAH), King Abdulaziz City for Science and Technology, Kingdom of Saudi Arabia, Award Number (12–BUI2620–02).

References

[1] Choi HK, Choi YC, Choi CS. Development and testing of precast concrete beam-to-column connections. Eng Struct 2013;56:1820–35.
[2] Vidjeapriya R, Jaya KP. Experimental study on two simple mechanical precast beam column connections under reverse cyclic loading. J Perform Constr Facil 2013;27:402–14.
[3] Vidjeapriya R, Jaya KP. Behaviour of precast beam-column mechanical connections under cyclic loading. Asian J Civil Eng (Build Hous) 2014;13:233–45.
[4] Ertas O, Ozden S, Ozturan T. Ductile connections in precast concrete moment resisting frames. PCI J 2006;5:2–12.
[5] Joshi MK, Murty CV, Jaisingh MP. Cyclic behaviour of precast RC connections. Indian Concr J 2005;79:43–50.
[6] Savoia M, Buratti N, Vincenzi L. Damage and collapses in industrial precast buildings after the 2012 Emilia earthquake. Eng Struct 2017;137:162–80.
[7] ASCE/SEI 7–10. Minimum design loads for buildings and other structures. Structural Engineering Institute-American Society of Civil Engineers, Reston, VA; 2010.
[8] DOD (Department of defense). Unified facilities criteria, design of building to resist progressive collapse, Department of Defense, U.S.; 2005.
[9] GSA (General Service Administration). Alternate path analysis & design guidelines for progressive collapse resistance. The U.S. General Services Administration; 2013.
[10] NBCC. National building code of Canada. Ottawa, Canada: National Research Council of Canada; 1995. p. 1996.
[11] IBC. International building code 2000. In: International Conference of Building Officials, Whittier, CA: International Code Council Inc; 2000.
[12] ISC. ISC Security criteria for new federal office buildings and major modernization projects. The Interagency Security Committee; 2001.
[13] Pearson C, Delatte N. Ronan Point apartment tower collapse and its effect on building codes. J Perform Constr Facil 2005;19(2):172–7.
[14] Almusallam TH, Elsanadedy HM, Abbas H, Alsayed SH, Al-Salloum YA. Progressive collapse analysis of a RC building subjected to blast loads. Struct Eng Mech 2010;36(3):301–19.
[15] Allen DE, Schriever WR. Progressive collapse, abnormal load, and building codes. Structural failure: modes, causes, responsibilities. In: Proc American Society of Civil Eng, New York; 1972.
[16] Robertson IN, Riggs HR, Yim SCS, Young YL. Lessons from hurricane Katrina storm surge on bridges and buildings. J Waterway, Port, Coastal, Ocean Eng 2007;133(6):463–83.
[17] Peakau OA, Cui Y. Progressive collapse simulation of precast panel shear walls during earthquakes. Comput Struct 2006;84:400–12.
[18] Almusallam T, Al-Salloum Y, Ngo T, Mendis P, Abbas H. Experimental investigation of progressive collapse potential of ordinary and special moment resisting reinforced concrete frames. Mater & Struct 2017;50:137.
[19] Allen DE, Schriever WR. Progressive collapse, abnormal load, and building codes, structural failure: modes, causes, responsibilities. New York: Proc American Society of Civil Engineers; 1972.
[20] Elsanadedy HM, Almusallam TH, Alharbi YR, Al-Salloum YA, Abbas H. Progressive collapse potential of a typical steel building due to blast attacks. J Constr Steel Res 2014;101:143–57.
[21] Baldridge SM, Humay FK. Reinforced concrete and secure buildings: progressive collapse. The structural bulletin series, concrete reinforcing steel institute, No. 2; 2004.
[22] Choi J, Chang D. Prevention of progressive collapse for building structures to member disappearance by accidental actions. J Loss Prevent Proc 2009;22:1016–9.
[23] Al-Salloum YA, Almusallam TH, Khawaji MY, Ngo T, Elsanadedy HM, Abbas H. Progressive collapse analysis of RC buildings against internal blast. Adv Struct Eng 2015;18(12):2181–92.
[24] Dat PX, Haiand TK, Jun Y. A simplified approach to assess progressive collapse resistance of reinforced concrete framed structures. Eng Struct 2015;101:45–57.
[25] Bao Y, Kunnath SK, El-Tawil S, Lew HS. Macromodel-based simulation of progressive collapse: RC frame structures. J Struct Eng-ASCE 2008;134(7):1079–91.
[26] Kang SB, Tan KH. Behaviour of precast concrete beam-column sub–assemblages subject to column removal. Eng Struct 2015;93:85–96.
[27] Alcocer SM, Jirsa JO. Strength of reinforced concrete frame connections rehabilitated by jacketing. ACI Struct J 1993;90(3):249–61.
[28] Ghobarah A, Aziz TS, Biddah A. Rehabilitation of reinforced concrete frame connections using corrugated steel jacketing. ACI Struct J 1997;94(3):282–94.
[29] Antonopoulos C, Triantafillou TC. Experimental investigation of FRP-strengthened RC beam-column joints. J Compos Constr 2003;7(1):39–49.
[30] Al-Salloum YA, Almusallam TH. Seismic response of interior beam-column joints upgraded with FRP sheets. I: Experimental study. J Compos Constr 2007;11(6):575–89.
[31] Alsayed SH, Al-Salloum YA, Almusallam TH, Siddiqui NA. Seismic response of FRP-upgraded exterior RC beam-column joints. J Compos Constr 2010;14(2):195–208.
[32] Al-Salloum YA, Siddiqui NA, Elsanadedy HM, Abadel AA, Aqel MA. Textile-reinforced mortar versus FRP as strengthening material for seismically deficient RC beam-column joints. J Compos Constr 2011;15(6):920–33.
[33] Da Fonseca T, de Almeida SF, de Hanai JB. Beam-to-column connection of a precast concrete frame strengthened by NSM CFRP strips. In: Proc of CICE 2010 - The 5th International Conference on FRP Composites in Civil Engineering, Beijing, China, Sept 27–29; 2010.
[34] Gopinathan MJ, Subramanian K. High performance and efficiency of joints in precast members. Int J Eng Technol (IJET) 2013;5(5):4002–9.
[35] de Freitas ST, Kolstein H, Bijlaard F. Lightweight reinforcement systems for fatigue-cracked orthotropic bridge decks. Struct Eng Int 2013;23(4):458–67.
[36] ACI Committee 318. Building code requirements for structural concrete and commentary. ACI 318-11, American Concrete Institute, Detroit, MI, USA; 2011.
[37] Sika. Datasheet for Sikadur®-31 – Thixotropic epoxy resin adhesive mortar; Sep 2004, 4p.
[38] ASTM. Standard test method for compressive strength of cylindrical concrete specimens. ASTM C39/C39M, American Society for Testing and Materials, West Conshohocken, PA, USA; 2010.
[39] ASTM. Standard test methods for tension testing of metallic materials. ASTM E8/E8M, American Society for Testing and Materials, West Conshohocken, PA, USA; 2009.
[40] ASTM. Standard test methods and definitions for mechanical testing of steel products. ASTM A370–16, American Society for Testing and Materials, West Conshohocken, PA, USA; 2016.
[41] Ngo T, Mendis P, Gupta A, Ramsay J. Blast loading and blast effects on structures – An overview. Electronic Journal of Structural Engineering (EJSE); 2007. p. 76–91 [special issue: Loading on Structures].
[42] NZS 4203: 1992. New Zealand Standard, Code of practice for general structural design and design loadings for buildings 1; 1992.
[43] CEB-FIP Model Code. Comité Euro-International du Béton. Trowbridge, Wiltshire, UK: Redwood Books; 1990. p. 1990.
[44] Malvar LJ. Review of static and dynamic properties of steel reinforcing bars. ACI Mater J 1998;95(5):609–16.
[45] ACI Committee 318. Building code requirements for structural concrete and commentary. ACI 318–14, American Concrete Institute, Detroit, MI, USA; 2014.
[46] Computers and Structures Inc. SAP2000 Ultimate 32-bit – version 17.2.0. CSI, Berkeley, CA, USA; 2015.
[47] Priestley MJN, Seible F, Calvi GM. Seismic design and retrofit of bridges. John Wiley & Sons Inc; 1996, 686p.
[48] Elsanadedy HM, Haroun MA. Seismic design guidelines for squat composite-jacketed circular and rectangular reinforced concrete bridge columns. ACI Struct J 2005;102(4):505–14.